ChemElectroChem

Review
doi.org/10.1002/celc.202300620

Chemistry Europe
European Chemical Societies Publishing

www.chemelectrochem.org

Insights into the Interfacial Charge Transfer Dynamics in Semiconductor–Molecular Catalyst Assemblies for Photo–induced CO_2 Reduction

Tamal Chatterjee,*[a, b] Beatriu Domingo-Tafalla,[a, c] Pablo Ballester,*[a, d] and Emilio Palomares*[a, d]

This mini–review summarises examples of photo and photoelectrochemical CO_2 reduction reactions (CO_2RR) using semiconductor–molecular catalyst–based hybrid assemblies in which studies of charge transfer dynamics were also performed. In these catalysts, the grand challenges are controlling ultra–fast one–electron charge separation and simultaneously governing its impact on the efficiency and product selectivity in the multielectron and multi–proton–assisted CO_2RR. In practice, several unwanted electron recombination processes occur in the femtosecond to millisecond timescale range impacting the overall catalysis efficiency. Titanium di-oxide (TiO_2) nanoparticle, mesoporous TiO_2 film, copper indium sulphide ($CuInS_2$) quantum dots were used as semiconductor materials, in turn rhenium (I) bipyridine, cobalt (II) terpyridine, cobaloxamine complex, and iron (III) porphyrins were investigated as molecular catalysts. The results of the charge transfer dynamic studies operating in such hybrid systems shed light on their charge accumulation processes, their rate constants for the intramolecular charge transfer processes and the decay lifetimes of the different excited state species that are produced. Moreover, a comprehensive understanding of the catalysts' charge transfer dynamics is crucial to identifying detrimental charge recombination pathways. These undesired pathways can be used as rational basis for improving the design of future multi–redox–driven hybrid catalysts.

1. Introduction

Inspired by Natural Photosynthesis, *Artificial photosynthesis* emerged as a compelling alternative to mitigate the adverse impact of anthropogenic CO_2 emission in the 21st century.[1] It promises to secure future global energy (~20 TW/year) for ~10 billion population by 2055,[2] without having to resort to non–renewable resources (fossil fuels). Artificial photosynthesis technology commits to the generation of *Solar Fuels* using sunlight and abundant H_2O and CO_2 molecules at ambient temperature and pressure conditions.[3] A paramount interest has been spurred globally in obtaining such artificial ecosystems with expectations to achieve higher efficiencies than natural photosynthesis. During natural photosynthesis, light–harvesting chlorophyll antenna complexes act as photosensitisers absorbing visible light. After that, ultrafast photoinduced charge separation occurs in the femtosecond (fs) to picosecond (ps) timescale.[4] Later, the excited electrons shuttle through an electron transport chain in nanosecond (ns) to microsecond (μs) timescale, and are finally transferred to suitable proteins for the generation of NADPH and ATP. During the dark reaction, NADPH, ATP, and CO_2 are combined to make sugars, but the involved reactions (Calvin cycle) take place at a slower (micro to millisecond (ms)) time scale. Overall, natural photosynthesis is a relatively inefficient process, with a maximum light-to-chemical energy conversion of ~3–6% only (C3 and C4 plants). Numerous energy conversion bottlenecks are responsible for this limitation.[5] Seeking to develop related molecular machinery for the light-induced artificial CO_2 reduction reaction (CO_2RR) requires a photosensitiser, as a light-absorbing unit, followed by charge-separation and transfer of the photoexcited electrons to the catalytic centre. CO_2 molecules bound to the catalytic centre would then be reduced to valuable chemicals.[6] Although Nature performs carbon fixation by converting CO_2 into complex sugar molecules containing multiple C–C bonds, in the artificial version, simply converting CO_2 selectively into any of the following chemicals (CO/HCOOH ($2e^-$), CH_3OH ($6e^-$), CH_4 ($8e^-$) or C_2H_5OH/C_2H_4 ($12e^-$)) via favourable proton–coupled electron transfer (PCET) reactions constitutes a challenging task.[7] The produced chemicals are valuable as alternatives to non–renewable resources (fossil fuels) or commodity chemicals used in the industry. Hence, obtaining an artificial cost–

[a] T. Chatterjee, B. Domingo-Tafalla, Prof. P. Ballester, E. Palomares
Institute of Chemical Research of Catalonia (ICIQ)-CERCA Avinguda Països Catalans 16, 43007 Tarragona, Spain
[b] T. Chatterjee
CSIR-Advanced Materials and Processes Research Institute (AMPRI), Hoshangabad Road, Bhopal, Madhya Pradesh, 462026, India
[c] B. Domingo-Tafalla
Universitat Rovira i Virgili (URV), Departament D'enginyeria electrònica, Elèctrica i Automatica, Avinguda Països Catalans, 43007 Tarragona, Spain
[d] Prof. P. Ballester, E. Palomares
Catalan Institution for Research and Advanced Studies (ICREA), Passeig Lluís Companys, 23, 08018 Barcelona, Spain
and
Institute of Chemical Research of Catalonia (ICIQ)-CERCA. Avinguda Països Catalans 16, 43007, Tarragona, Spain
E-mail: tchatterjee@iciq.es
pballester@icq.es
epalomares@iciq.es

effective, stable catalytic system with good light harvesting properties for CO_2RR efficiency is still in the prime agenda of most studies in the area.

Photochemical (PC) and photoelectrochemical (PEC) CO_2 reduction reactions using different types of metal oxide (*n*-type TiO_2, ZnO, NiO, Cu_2O, etc.),[8] carbonaceous materials (g-C_3N_4),[9] quantum dots[10] (CdS, CdSe) and other types[11] (*p*-type Si, GaP, GaAs, ZnS, etc.) of semiconductor materials are not new. They have been studied for a couple of decades. In semiconductor materials, the photogenerated excited electrons can reduce surface–adsorbed CO_2 molecules, while the holes can oxidise water to O_2 or promote any other organic oxidation reactions (Figure 1). However, photo–excited electrons and holes are prone to recombine at a much faster timescale (ps to ns) than the timescale for their migration to the semiconductor surface and consumption in CO_2RR (ns to μs).[12] This recombination phenomenon significantly reduces the overall photocatalytic efficiency. Moreover, the standard reduction potentials of CO_2 (Figure 2b) indicate a relatively low thermodynamic barrier for the production of several reduced products along with the competitive hydrogen evolution reaction (HER).[13] Thus, the use of semiconductor materials alone, in the role of light–harvesting and catalyst, results in a significant challenge for controlling the CO_2RR selectivity. On the other hand, molecular catalysts based on earth–abundant 3d transition metal complexes (Fe, Co, Ni, Cu, etc.) are well known for their efficiency in metal–centred electrochemical CO_2RR that are selective in terms of produced products.[14] Still, catalysts based on molecular metal complexes usually suffer from medium to long–term stability issues. However, they possess a subtler advantage that is associated with the synthetically easy tuning of the ligand's framework causing favourable electronic and steric effects towards the CO_2RR. In this vein, a handful of literature reports describe the use of Ni-cyclam, Re- and Ru-bipyridine and terpyridine, Fe- and Co-porphyrin, and Co-phthalocyanine, Co-quaterpyridine complexes for the CO_2RR. These reports also include mechanistic studies of the reaction supported by experimental and theoretical results.[15] The individual limitations of the CO_2RR associated with semiconductor materials and molecular catalysts alone can be partially overcome by constructing hybrid systems combining molecular catalysts with semiconductors (Figure 2). Developing such hybrid assemblies mimicking natural photosynthetic systems is a complex and demanding task. To address the issue, many research efforts are actively underway by combining narrow–band gap semiconductors with integrated molecular catalyst. The hybrid system fabrications more vastly explored are based on the immobilisation and anchoring of the molecular catalyst to the semiconductor in addition to the catalytic efficiency, product selectivity, and stability of the prepared hybrid systems for the CO_2RR.[16] However, except for a few reports, the detailed investigation of the vital interfacial charge transfer processes occurring in the hybrid systems have not been reported. During the light–induced CO_2RR, the interfacial charge transfer processes occurring in the hybrid

Tamal Chatterjee obtained his B.Sc and M.Sc in Chemistry at the University of Burdwan and his Ph.D. in inorganic chemistry at the IIT Bombay, India. After a short industrial R&D stay in India, he joined the group of Prof. Marc Robert at the University of Paris as a postdoc with a Make Our Planet Great Again grant (France). In 2021, he moved to the group of Prof. Emilio Palomares at ICIQ, Tarragona. He is recipient of Beatriu de Pinós Grant AGAUR, Catalonia, (Spain). His current research focus on the interface of electrochemistry, photochemistry, and molecular catalysis for solar fuel production.

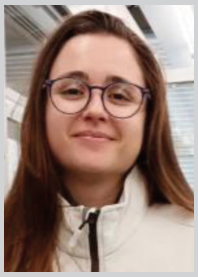

Beatriu Domingo is a PhD student in the Prof. Emilio Palomares group at the Institut Català d'Investigació Química (ICIQ), in Tarragona (Spain), under an FPI fellowship from the spanish Ministerio de Ciencia e Innovación/ Agencia Estatal de Investigación. In 2019 she graduated in Nanoscience and Nanotechnology from the Autonomous University of Barcelona and the University of Technology Sydney (UTS). Afterwards, she carried out her Master's thesis in the Institut de Ciència de Materials de Barcelona in collaboration with the Institut de Bioenginyeria de Catalunya under the supervision of Dr. Nora Ventosa. Her current research is focused on the design, synthesis and characterization of hybrid nanomaterials for (photo)electrochemical CO_2 reduction

Pablo Ballester, completed his Ph.D. in 1986 under the direction of Prof. Ramon Mestres at the University of the Balearic Islands (UIB). He worked as a postdoctoral fellow with Prof. Julius Rebek, Jr. at the University of Pittsburgh and the Massachusetts Institute of Technology (MIT), and with Prof. José M. Saá at the UIB. In 1990, he joined the Chemistry Department of UIB as Assistant and rose to the rank of Associate Professor. In 2004, he was awarded an ICREA Research Professorship and moved to the ICIQ as a group leader. In 2021, he was elected Member of the European Academy of Science. His current research interests are in the areas of molecular self–assembly, molecular recognition, supramolecular catalysis and artificial photosynthesis.

Dr Emilio Palomares is an ICREA Professor and group leader at ICIQ who became Director of the Institute in 2020. He has extensive experience designing and synthesizing energy materials and constructing third–generation solar cells of different natures, such as organic, quantum dot, dye-sensitized, or perovskite–based. He was awarded in 2009 with an ERC Starting Grant in 2023 and an ERC Advanced Grant. Prof. Palomares has co–authored more than 200 peer–reviewed scientific papers on molecules and materials for energy-related devices.

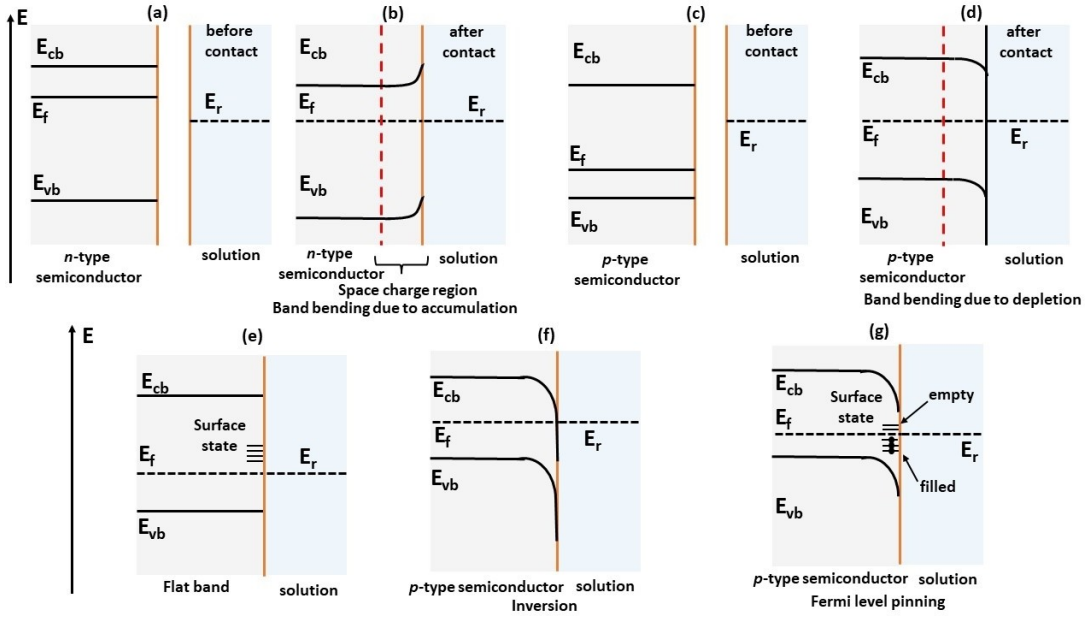

Figure 1. Band diagram for semiconductor/electrolyte interfaces without bandgap excitation. (a) and (b) *n*-type semiconductor (accumulation), (c) and (d) *p*-type semiconductor (depletion), (e) flat band, (f) inversion, and (g) Fermi level pinning. The band potentials are varied with the distance from the surface of the semiconductor to the bulk. E_{vb} = Valence band, E_{cb} = Conduction band, E_f = Fermi level, E_r = redox species at the solution/electrolyte, E_{ss} = Surface state in the semiconductor.

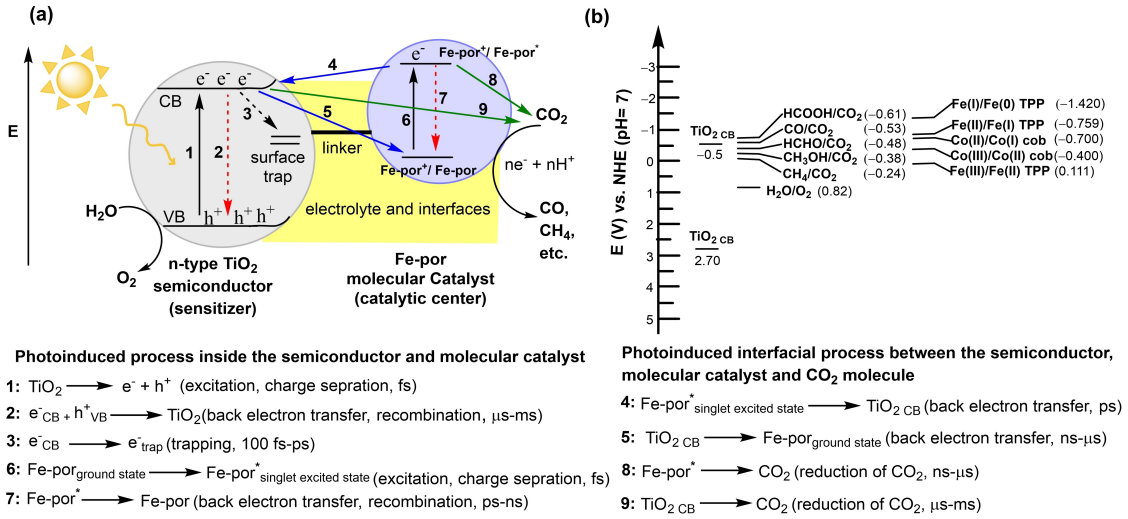

Figure 2. (a) Schematic representation of the charge transfer processes (process **1**–**9**, along with the tentative time scale) in a semiconductor–molecular catalyst system during the photo–induced CO_2RR. The diagram takes the mesoporous TiO_2/Fe-porphyrin (**Fe**–**por**) as a model system. (b) The VB and CB band position of TiO_2, standard reduction potentials of products deriving from CO_2-reduction, and water oxidation are depicted. On the extreme right side, the Co and Fe centred reduction potentials (vs NHE) of the Cobalt diamine–dioxime (**Co**–**cob**) and Iron tetraphenyl porphyrin (**Fe**–**TPP**) complex are depicted. Data are taken from the literature, where the CV of **Fe**–**TPP** is recorded in DMF with $TBAPF_6$ as a supporting electrolyte, and the CV of **Co**–**cob** is registered after attaching it onto ITO in ACN with $TBAPF_6$ as a supporting electrolyte. It is important to note that the Fe and Co–based redox potentials are not measured at pH = 7; it is shown to get an idea about the redox levels concerning other values as depicted.

systems are directly related to their efficiency and catalytic performance. In short, interfacial charge transfer processes are a fundamental aspect of the hybrid catalytic systems and cannot be overlooked. Following light irradiation and charge separation, a unilateral interfacial charge transfer process from the semiconductor conduction band edge to the metal centre of the molecular catalyst produces a low oxidation state at the metal centre which is mandatory for the subsequent CO_2 catalytic reduction.[17] Model hybrid systems with suitably matching band edge and metal centre with multi–redox potentials can be constructed for the validation of photo–induced CO_2RR. In the hybrid systems, it is possible to investigate one–electron charge separation events, occurring at the fs to ps time scale, as well as the ultimate multi–electron and multi–proton–assisted CO_2RR. The groups of Durrant and Reisner carried out studies of the interfacial charge transfer

dynamics and CO_2RR using hybrid–catalytic systems composed of: a) titanium di-oxide (**TiO_2**) nanoparticles/[Re(I)(2,2'-bipyridine-4,4'-bisphosphonic acid)$(CO)_3$(3-$CH_3C_5H_4N$)] (**Re–bpy–pic**) (Figure 3d), and b) mesoporous **TiO_2**/[Co(II) terpyridine/cobaloxamine] complex (**Co–ter/Co–cob**) (Figure 3b).[18] The Wiess group also reported related studies with a hybrid catalytic system of copper indium sulphide (**$CuInS_2$**) quantum dot (QD)/Fe(III)-Tetra (*p*-N,N,N,trimethylanilinium) porphyrin **Fe–TMA**) (Figure 3c).[19] More recently, our group investigated two porphyrin-based catalytic hybrid systems in which Fe(III)-5-(4-carboxyphenyl)-10,15,20-tris (4-pentylphenyl) porphyrin (**Fe–por**) and Fe(III)-protoporphyrin IX (**Hemin**), respectively, were coupled to mesoporous TiO_2 (Figure 3a).[20] This review summarises the results obtained in the above–mentioned reports, describing pertinent factors affecting the CO_2RR as outcomes of various charge transfer events. We sought to correlate the catalytic properties of the investigated hybrid systems for the CO_2RR with the results obtained in the characterization of their interfacial charge transfer processes.

2. Energetics of semiconductor–solution interfaces

Interfacial redox reactions occurring at the semiconductor–solution interfaces are crucial in photoelectrochemical CO_2RR. Commonly, they are explained using the energy band model.[21] Pioneering work by Bartten and Garret, Marcus, and Gerischer (Gerischer Model) in the 1960s led to the foundation of semiconductor electrochemistry and photoelectrochemistry.[22] However, the energy band theory describes the states of electrons in solid-state physics of semiconductors and interfaces of two solids (e.g., *p* and *n*-type semiconductor) rather than in solid–solution interfaces. Suppose a semiconductor is placed in contact with a solution/electrolyte, depending on the Fermi energy (E_f) level in the semiconductor and the reduction potential (Er) of the redox active species in the electrolyte, electric current flows across the junction until electronic equilibration (E_f=E_r) is reached (Figure 1a and 1b).[21,23] The electrolyte redox potential remains essentially fixed due to its presence in significant large excess compared to the electrons or holes at the surface of the semiconductor.

The transfer of electric charges at the semiconductor–electrolyte junction results in a region where charge distribution differs from that of the bulk material; this area is called the *'space–charge region'* (Figure 1b and 1d). On the semiconductor side, the accumulation of electrons generates a negatively charged region near the space-charge area, which causes band bending. The nature of the band bending depends on the Fermi level of the semiconductor (*n*-type semiconductor, Figure 1a and 1b and *p*-type semiconductor, Figure 1c and 1d). The negative charges accumulated along the semiconductor side get balanced by the rearrangement of the ions within the double layer region (Helmholtz and Gouy–Chapman layer) of the electrolyte. This charge redistribution gives rise to an electric field at the space–charge region. For an ideal semiconductor, the charge redistribution varies with the distance from the interfaces to the bulk. Therefore, a parabolic variation in the potential occurs, and the energy of the electrons and holes gets modified at the space–charge region.

Light absorption triggers the separation of electron–hole pairs in semiconductors; the charge separation taking place at the space–charge region occurs more efficiently than in the semiconductor bulk. This greater efficiency is attributed to the presence of the electric fields, which dictate the migration of the electron towards the semiconductor surface and the hole towards the bulk regions of the material, thereby lowering electron–hole pair recombination rates.[24] The probability of the electron–hole pair separation at the space–charge region varies with the width of the area, dopant concentration, and applied external bias voltage during the photoelectrocatalysis. If the redox level of the electrolyte becomes equal to the Fermi level of the semiconductor, there is no excess charge on either side of the interface. Then, the Fermi level of the semiconductor is defined as *flat band potential* (E_{fb}) (Figure 1e). To counterbalance the band bending, an external potential is applied to the semiconductor/electrolyte junction resulting in the flattening of the valence and conduction bands. The applied potential is called the flat band potential. The value of the flat band potential can be determined from the Mott–Schottky plot. That is measuring the capacitance (C) of the semiconductor/electrolyte junction upon applying different voltages (V) and plotting the data ($1/C^2$ vs. V). An alternative situation may arise when the charge distribution (for example, electron depletion) at the space-charge region falls below the intrinsic Fermi level of the semiconductor. Under such circumstances, an *inversion layer formation* takes place (Figure 1f) provoking that a *p*-type semiconductor behaves as a *n*-type at the surface. Nevertheless, *inversion layer formation* in photoelectrocatalysis studies is rare but more common in solid-state interface studies.[25]

Using the band model described above, the dependence of the applied potential on band bending at the interface, width of the space–charge region, and photocurrent efficiency can be explained; however, the model is a simplification and does not consider the surface states of the semiconductor. In reality, most semiconductors (e.g., TiO_2, *p*-Si, etc.) contain redox–active surface states; their presence changes the charge distribution at the semiconductor/electrolyte interface exhibiting a non-ideal behaviour.[24] Electrochemical methods such as cyclic voltammetry and impedance spectroscopy can be used to characterise such electronic states. When surface states are occupied (E_{ss}, surface state energy), charges develop across the semiconductor surface, and a drop of potential across the interfaces is observed. As a result, when E_F~E_{ss}, the effect of the externally applied voltage on band bending deviated from the prediction based on the ideal band model. The presence of surface states in high density can 'pin' the Fermi level (*Fermi level pinning*) near the centre of the band gap, resulting in band bending in the semiconductor independent of the redox species (Er) present in the electrolyte/solution (Figure 1g). Until all surface states are completely occupied (filled) or unoccupied (unfilled) with electrons, a non–ideal variation of the Fermi levels with the external voltage prevails.[26] This phenomenon directly

impacts in the interfacial electron transfer and the measurement of its dynamics during photoelectrochemical studies. Below, we will describe better the phenomenon using adequate examples.

So far, substantial attention was given to studying semiconductor/electrolyte interfaces for solar cells based on a one–electron redox mediator. However, multi–electron transfer catalysis, such as those used in CO_2RR, received little attention. Very recently, several research groups started to dig into this and present–day developments created an urge for deep diving in the study of interfacial charge transfer processes in photo–induced reduction reactions producing solar fuels. Surendranath, Hammes–Schiffer, and co–workers showed that when Co(II) TPP was immobilised on a graphitic electrode, with applied potential, a Co(III) hydride species having an energy below the Fermi level of the graphite electrode was formed.[27] The species was obtained via a concerted PCET mechanism in aqueous solution, by-passing the typical Co(II/I) redox process, before leading to the cobalt hydride. They suggested the existence of a band–to–bond electron redistribution from the delocalised graphitic band state to the Co(II) d–orbital–based delocalised orbital. Progressing further, Mayer proposed the use of surface-H bond dissociation free energies (BDFE) scales to explain interfacial PCET-assisted redox reactions instead of the typical band–energy–based scales.[28] He also discussed the limitations of BDFE–based models and the practical difficulties encountered in obtaining H-bonded surface energies of the complex in a range of semiconductor materials. Keller et al. reported photoelectrochemical multi–electron reduction processes at the interfaces of hydrogen–terminated *p*-Si with methyl viologen (MV^{2+}) and ruthenium bipyridine $[Ru(bpy)_3]^{2+}$ complexes in acetonitrile.[29] MV^{2+} undergoes two one–electron transfer processes (−0.84 V and −1.27 V vs. ferrocene ($Fc^{0/+}$)), and $[Ru(bpy)_3]^{2+}$ experiences three Ru centre–based one–electron reductions (−1.76 V, −1.96 V, −2.22 V, vs. $Fc^{0/+}$). Noticeably, the two MV^{2+} reduction processes fall within the band gap of *p*-Si, however, the three Ru–centred reductions are energetically higher than the conduction band energy. In any case, kinetics and spectroscopic studies indicated the facilitation of both MV^{2+} and Ru centre reduction processes owing to charge accumulation, charge depletion, and the formation of an inversion layer at the semiconductor interfaces. This example provoked a cautious investigation on the surface electron potentials at semiconductor–electrolyte junctions in order to achieve multi–electron transfer processes in hybrid catalysts. At the same time, it demonstrated that the assumption of fixed energies for band edge positions for interfacial charge transfer processes is limited. Clearly, the Ru-centred reductions were expected to be highly inefficient energetically because their potentials were more negative than that of the conduction band edges of the semiconductor ($E_{cb} = -1.4$ V vs. $Fc^{0/+}$). Hence, the straightforward application of the conventional band structure model at the semiconductor/electrolyte interfaces to explain interfacial charge transfer processes in multi–electron transfer catalysis was challenged. The explanation and understanding of these processes demand a careful study of the charge separation and the interfacial charge transfer processes in semiconductor–molecular catalysts–based hybrid systems. In this vein, the control of the ligand's electronic structure offered by molecular catalysts plays a significant role in governing charge separation, charge accumulation within the space-charge region, and the interfacial charge transfer processes occurring under the CO_2RR condition.

3. Measurements and schematics of the photo–induced charge transfer processes in a semiconductor–molecular catalyst assembly

The interfacial charge transfer kinetics depends on the semiconductor–molecular catalyst redox potentials and associated photoelectrochemical conditions. From the thermodynamic viewpoint, the difference in the energy levels across the interfaces drives the interfacial charge transfer from the semiconductor to the molecular catalyst unit. The conduction band (CB) energy of the semiconductor must be more negative than the redox potential of the molecular catalyst used in the CO_2RR. In turn, the redox potential of the molecular catalysts should be more negative than those of the different products deriving from CO_2 reduction (Figure 2a and 2b). Generally, the standard redox potentials of the products deriving from CO_2 reduction are typically less negative than the CB energy of common metal–oxide, carbon–based, and quantum dot–based semiconductors.[30] However, aberrant mismatches between the energy level of the semiconductor CB and multi–electron–mediated metal redox potentials (mainly, the 2nd and 3rd reduction of the metal centre) of molecular catalyst are common. Facile transfer of the 2nd and 3rd electrons becomes energetically unfavourable for the CB electrons depending on the nature of the charge accumulation at the interface. However, transferring high–energy, non–thermal hot electrons could also drive such reduction processes. The interfacial hot electron transfer might be more efficient due to electron–phonon solid interactions.[31] Hence, this anomaly in energy levels between the semiconductor and the molecular catalysts often becomes detrimental to the overall efficiency of the photoinduced catalytic process. The relative difference between the CB energy of the semiconductor and the redox potentials of the molecular catalyst should be the starting point in choosing the pair. The redox potentials of the molecular catalyst can be measured by cyclic voltammetry (CV) and differential pulse voltammetry (DPV). However, the obtained potential values could be altered upon the molecular catalysts' attachment to the semiconductor surface yielding the hybrid system. The CB and VB band energies of semiconductors can be determined by combining electrochemical studies, X-ray Photoelectron Spectroscopy (XPS), and Ultraviolet Photoelectron Spectroscopy (UPS) with theoretical calculations.[12] In the context of CO_2 reduction, the valence band (VB) redox energy (holes, oxidizing in nature) of the semiconductor does not directly participate in the catalytic cycle. However, photogenerated holes in the VB can be efficiently scavenged using sacrificial electron donors (also called hole scavenger). This process is beneficial for

obtaining extremely long–lived electrons in the CB.[32] The long–lived CB electrons maximize the rate of photoinduced electron transfer into the molecular catalyst centre. The choice of the hole scavenger agents depends on the VB energy level of the corresponding semiconductor material; commonly, trimethylamine (TEA), triethanolamine (TEOA), methanol, and ascorbic acid are used as hole scavengers for CO_2RR.[33] Generally, during the CO_2RR, the VB redox equivalents (holes) is involved in water oxidation. The thermodynamics and kinetic aspects of the interfacial (semiconductor-molecular catalyst) charge transfer processes impact on the performance of photoinduced CO_2RR. The size, morphology, and intrinsic structure band of the semiconductor, as well as the redox potential of the molecular catalyst, the electrolyte, the pH of the solution, and the intensity of the light markedly influence the kinetics of the process.[16,17a] Charge transfer studies under CO_2RR conditions using model systems are necessary to evaluate all these parameters and better understand the rate constants (dynamics) of the photoinduced intramolecular charge transfer processes, as well as lifetime decays of the excited state species having different electronic energy.

The photoinduced process in the semiconductor–molecular catalyst assembly initiated with an ultrafast charge separation step.[12] Then, the reducing equivalent (electron) at the semiconductor has to be transferred to the interface to be available for direct CO_2RR or to the molecular catalyst to produce a reduced metal state. However, if the molecular catalyst (e.g., metalloporphyrins, metallophthalocyanines) absorbs light strongly in the visible region, it may produce the corresponding excited singlet and triplet states without any interfacial charge transfer. These directly produced excited states of the molecular catalyst can be involved in additional charge transfer processes with the CB or VB of the semiconductor (Figure 2a). Time–resolved transient absorption spectroscopy (TAS) has been widely employed to monitor such ultrafast interfacial charge transfer processes.[34] With the advent of ultrafast lasers, it is possible to measure charge–transfer kinetics in the femtosecond to the second timescales by employing suitable TAS setups. During the charge transfer process, the reduction of the metal centre in the corresponding molecular catalyst [e.g., Co(II) complex to Co(I) complex] can be probed by means of in–situ UV-vis spectroelectrochemical (SEC) measurements. This technique exploits the diagnostic UV-vis absorption spectra of the different states of the metal oxidation (e.g., Co(II) and Co(I)) in the corresponding metal–complex unit.[18b] Photoluminescence spectroscopy (PL), is another essential tool that can be employed in the study of electron transfer and hole transfer processes in photocatalytic reactions. In this latter case, the electronic structure of the semiconductor is the one that is probed.[35] PL spectroscopy is also convenient for examining the role of the semiconductor trap states. The trap–states related emission and luminescence generated by the recombination of excited electrons and holes are measured.

Figure 2a depicts the schematic representation of the photoinduced charge transfer processes that are present in the TiO_2–Iron porphyrin-based hybrid system during CO_2RR.[20] The TiO_2–Iron porphyrin hybrid assembly is used as model system owing to: a) the widely studied properties of the mesoporous TiO_2 as photosensitiser and b) the well–known characteristics of iron-porphyrins as promising molecular catalyst for selective CO_2 to CO reduction. The tentative time scales of the different charge transfer processes ranging from fs to s timescale are also indicated in the figure 2. The separation of the initially photoinduced electron–hole pairs, processes **1** and **6** in Figure 2a, in TiO_2 and Fe-porphyrin (**Fe–Por**), respectively, occur in the fs timescale. These are immediately followed by a series of recombination processes occurring at different time scales. Namely, back electron transfer in **TiO_2** (process **2**, in μs-ms) and **Fe–por** (process **7** in ps-ns), and trapping of the charges on the semiconductor (process **3** in fs-ps). Processes **4** (ps) and **5** (ns-μs) are denoted for the interfacial charge transfer between the **Fe–Por** and **TiO_2** components of the hybrid assembly.

The transfers of charge to the absorbed (bound) CO_2 molecule are represented by processes **8** and **9**, which take place at a much slower time scale (ns-ms). From Figure 2, it is clear that the **TiO_2** CB energy level is not thermodynamically favourable to drive the reduction of the molecular catalyst up to the Fe(I) or Fe(0) states that are necessary for CO_2 reduction. In such scenario, slowing down the recombination process **4** will maximize the use of the electrons in the **TiO_2** in driving the multi–redox reduction of the molecular catalyst metal centre. It will also benefit the interfacial charge transfer efficiency and accelerate the CO_2RR. This observation is pertinent for the band energy levels of **TiO_2** and the different redox states of **Fe-porphyrin**. However, the results of the interfacial charge transfer kinetics studies are expected to be different in each semiconductor and molecular catalyst hybrid assembly (Figure 3). These results can be primarily used in accelerating interfacial charge transfers, enabling multi–redox reactions and identifying detrimental steps concerning the merit of the CO_2RR. Therefore, gaining insights into the interfacial charge transfer dynamic processes operating in different semiconductor-molecular catalyst assemblies is essential for the advancement in the area of CO_2RR. For this reason, we considered it a timely topic worth to be reviewed.

4. Examples of interfacial charge transfer studies under CO_2RR catalysis using semiconductor–molecular catalysts hybrid assemblies

In the context of photoelectrochemical CO_2RR, the charge transfer dynamics occurring in semiconductor–molecular catalyst–based hybrid assemblies are quite complex owing to many variables. To begin with, we will present a brief discussion on charge transfer studies performed using molecular catalysts and semiconductors, separately. The results of these studies are pertinent and highly relevant to better understand the timescales of more complex photoinduced processes occurring in the hybrid assemblies. Aukauloo and co-workers reported a covalently connected photosensitizer-molecular catalysts system comprising a ruthenium (II) tris bipyridine (**Ru–bpy**) and an iron (III) porphyrin (**Fe–OMe–por**) unit for the photochemical CO_2 reduction.[36] In acetonitrile/water (6:4 v/v), the **Ru–bpy**/**Fe–OMe–por** molecular dyad exhibited competition

for photon absorption between its two components and an efficient energy transfer occurred from the excited singlet Ru species to the singlet porphyrin, which in turn significantly quenched (shorter than 20 ns) fluorescence lifetime for the **Fe–OMe–por** unit (heavy metal effect from the Fe). As a result, the covalent **Ru–bpy/Fe–OMe–por** system did not show any photocatalytic CO_2 reduction activity as catalytically active Fe(0) reduction state of the porphyrin was never attained. The groups of Reisner and Hammarström also reported an improved CO_2 to CO photocatalytic reduction activity using a series of Co and Ni terpyridine complexes, as well as tetra–alkylammonium Fe-porphyrin derivatives, that were self–assembled in the membranes of liposomes together with an amphiphilic ruthenium dye acting as photosensitiser.[37] The functioning of the supramolecular systems required the use of sodium ascorbate as sacrificial electron source. Time–resolved and steady–state spectroscopy revealed that despite the lower photoinduced charge separation quantum yield (Φ_{ET}) of the Ru dye inserted in the liposome (6% with respect to 35% in homogenous solution), the insertion of the two molecular components (metal complex catalyst and dye sensitizer) in the lipid membrane slowed down the recombination process favouring a long–lived charge–separated state. The efficient first electron transfer (k_{ET}~10^{10} $M^{-1}s^{-1}$) process from the excited Ru dye to the closely spaced Ni-complex and the large lifetime of the resulting charge–separated state boosted the CO_2RR catalysis. Weiss and co–workers used colloidal **$CuInS_2$** quantum dots (QD) to photosensitize an **Fe–TPP** catalyst to achieve photocatalytic CO_2 to CO reduction.[10] Upon 450 nm photoexcitation, three ultrafast successive electron transfer processes occurred from the **$CuInS_2$** QD to Fe–TPP porphyrin yielding the Fe(0) reduction state of the active catalyst. The TAS study revealed that the first two [Fe(III) to Fe(II) and Fe(II) to Fe(I)] electron transfers happened in $<$200 fs and demonstrated that the photoreduction of [Fe(I) to Fe(0)] was five–fold slower than the photoreduction of [Fe(II) to Fe(I)]. Furthermore, the use of N,N,N′,N′-tetramethyl-*p*-phenylenedi–amine (TMPD) as a sacrificial electron donor regenerated the **$CuInS_2$** QD's ground state within 700 ps sustaining the catalytic cycle for 40 h. Recently, our group investigated the accumulation and lifetime of photogenerated electrons in mesoporous **TiO_2** by controlling the applied bias in the presence of CO_2. By probing the transient signal of the **TiO_2** conduction band electrons using TAS, we observed a decrease in the accumulation of charges in the **TiO_2**, under an applied bias, when CO_2 was present. This result indicated that electron transfer processes from the **TiO_2** photocathode to the bound CO_2 was taking place (Figure 6a, black and red trace).[20] Moving from N_2 to CO_2 atmosphere, under 355 nm laser excitation with an applied voltage bias (0 to −0.8 V vs. Ag/AgCl), the **TiO_2** film exhibited a decrease in transient absorption (at −0.5 V by 35%). In addition, the lifetime of the photogenerated electrons also diminished (at −0.5 V by 50%) (Figure 6b, black and red trace). The photogenerated **TiO_2** electrons furnished the CO_2RR producing CO and CH_4 as reduction products either in presence or absence of an external voltage bias.

On the other hand, under typical electrochemical conditions, the same **TiO_2** electrode required a threshold applied voltage of at least −1.8 V to induce the CO_2RR.[20] Taken together, the results obtained in the above–mentioned studies suggested an advantage in using photoinduced electrons for the CO_2RR. They induced a better catalytic activity at lower overpotential values. In the following section, we will describe the effects exerted on the charge transfer dynamics of the reported semiconductor–molecular catalyst systems for CO_2RR (Figure 3).

4.1. Effect of the linker/grafting method

The assembly of the hybrid photocatalytic systems used for the CO_2RR are based either on the formation of ester linkages between the hydroxyl groups of **TiO_2** and the –PO_3H/–COOH groups of the molecular catalysts or the establishment of coulombic interactions between the cationic molecular catalysts and the anionic groups of the semiconductor (Figure 3).

The **Co–ter/Co–cob** complexes (on **TiO_2** films) and **Re–bpy–pic** (on **TiO_2** nanoparticles) were covalently attached via a tridentate ester–linkage of their phosphonic acid groups.[18] In contrast, the **Fe–por** and **Hemin** were immobilized on **TiO_2** films using an ester–linkage between the carboxylic acid groups of the former and the hydroxyl groups of the later.[20] In the coulombic self-assembly, the surface of **$CuInS_2$** quantum dots was modified by reaction with the thiolate end of 3-marcaptopropanoic acid (MPA) linker. The carboxylate ends of the linker pointing away from the surface interacted with the positively charged quaternary ammonium groups of the **Fe–TMA**.[19]

The immobilisation of the molecular catalysts onto the **TiO_2** semiconductor surfaces was confirmed by monitoring the P=O, P–O or C=O, and C–O stretching frequencies in their IR spectra and the Ti 2p, O 1s, and Fe 2p bands in the XPS counterparts. In any case, irrespective of the catalysts grafting procedure for assembly of the hybrid systems, the anchoring strategy aimed at achieving efficient energy and redox transfer processes, providing long–term stability to the molecular catalysts incorporated on the semiconductor surface under photo–irradiation and the applied reductive bias for CO_2RR. Under photocatalytic conditions, **TiO_2–Re–bpy–pic** showed a good turnover number (TON) for CO formation, in the presence of TEOA as sacrificial agent and in DMF solution under light irradiation for 24 h ($\lambda>420$ nm). Similarly, the **$CuInS_2$–Fe–TMA** hybrid system furnished CO in water with light irradiation during 30 h ($\lambda=450$ nm).[18a,19] Using photoelectrochemical conditions, **TiO_2–Hemin** and **TiO_2–Fe–Por** also produced CO; the **TiO_2–Hemin** assembly remained stable up to −1.5 V (vs. Ag/AgCl), whereas the **TiO_2–Fe–Por** analogue became unstable at an applied potential of −0.5 V (vs. Ag/AgCl).[20] Most likely, the difference in the number of anchoring groups of the two porphyrins was responsible for the dissimilar stability of the two hybrid assemblies. **Hemin** contains two carboxylic acid functions, but the **Fe–Por** was equipped with only one –COOH group as *p*-phenyl substituent. Thus, the nature and structure of the linker units had a pronounced effect on the catalysis efficiency and stability of the hybrid assemblies for the CO_2RR. In contrast, the results of the TAS studies of the two slightly different hybrid assemblies (**TiO_2–Hemin** and **TiO_2–Fe–Por**) assigned similar timescale (fs-ms) to their charge separation and accumulation processes.

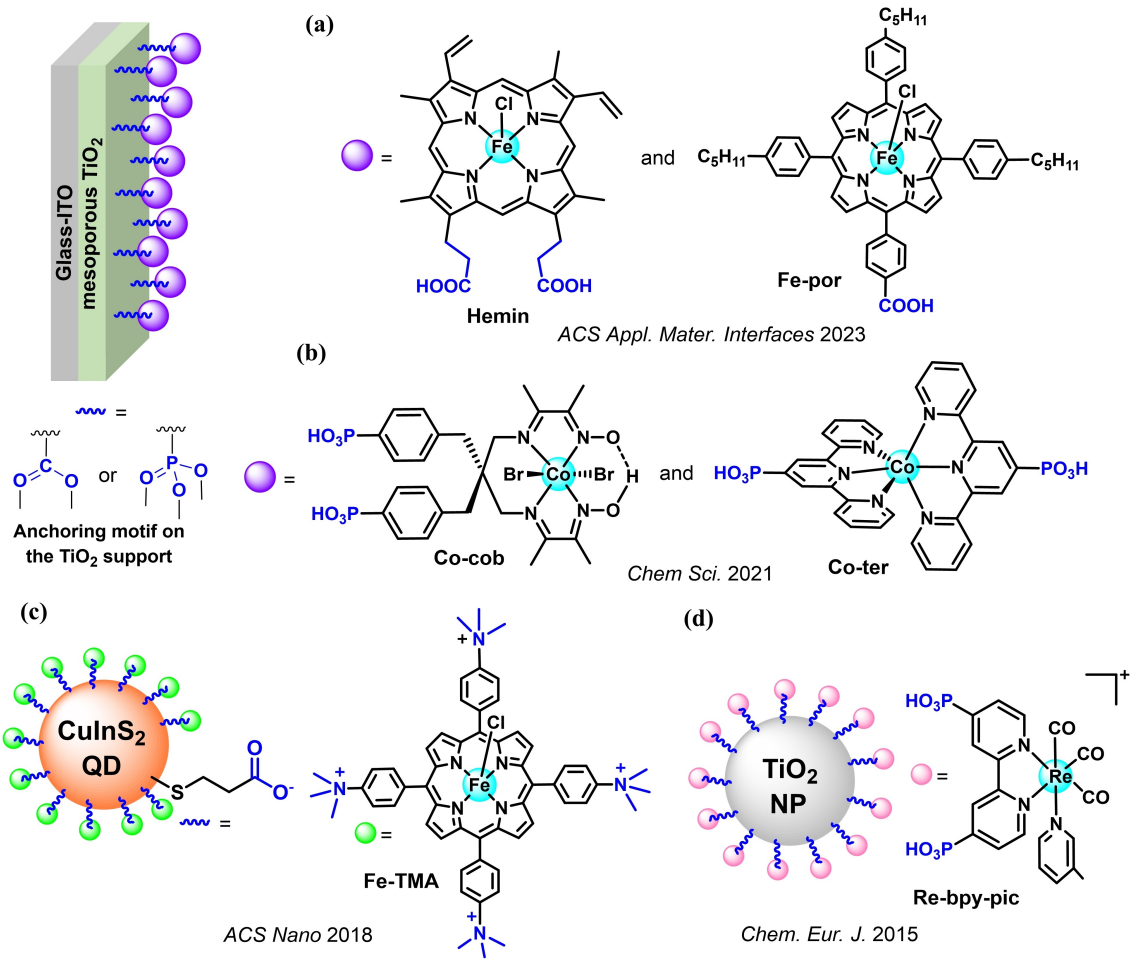

Figure 3. Examples of semiconductor–molecular catalyst systems (a) **TiO_2–Hemin**, **TiO_2–Fe–Por**; (b) **TiO_2–Co–cob**, **TiO_2–Co–ter**; (c) **$CuInS_2$–Fe–TMA**; (d) **TiO_2–Re–bpy–pic** studied for the photo-induced CO_2 reduction and interfacial charge transfer processes. The structures of the abbreviated molecular complexes are shown in the Figure.

4.2. Charge transfer processes driving the multi-redox CO_2 catalysis

Under photochemical conditions, the reduced **Re–pic$^-$** species was identified as the catalytically active intermediate species in the **TiO_2–Re–bpy–pic** hybrid assembly. This species exhibited a characteristics transient absorption signal at $\lambda_{max} = 500$ nm.[18a] Under N_2 atmosphere and in DMF solution (containing 1 M TEOA), the decay of the transient absorption of the **Re–pic$^-$** species assigned a larger lifetime in the hybrid-assembly **TiO_2–Re–bpy–pic** ($t_{50\%} > 1$ s) than for the free **Re–bpy–pic** ($t_{50\%} > 60$ ms) complex diffusing in solution (Figure 4a). In the presence of CO_2, the transient decay of the absorption of **Re–P_{pic}^-** followed a biphasic behaviour, with a first fast component decay in the 1–10 ms timescale and a slower component decay in the range of 100 ms–1 s timescale (Figure 4b).

The faster decay in presence of CO_2 was assigned to the interaction between CO_2 molecules and the active **Re–P_{pic}^-** species. Based on spectroscopic results and theoretical calculation studies, the authors proposed that, first **Re–P_{pic}^-** binds CO_2 in a ~400 ms timescale followed by a second electron transfer taking place on the **Re–pic–CO_2** adduct. The kinetics of the second reduction step was not observed in TAS measurement. This second electron transfer is mediated by the sacrificial electron donor leading to the generation of CO and H_2O. In the electrostatically coupled **$CuInS_2$–Fe–TMA** hybrid system, the study of the dynamics of the photoinduced electron transfer process from the MPA-capped **$CuInS_2$** QD to **Fe–TMA** was carried out by means of TAS and time–correlated single photon counting (TCSPC).[19] The features of the ground state bleach (GSB) for the **$CuInS_2$** QD suggested a decay of the excited electrons via intrinsic pathways and through an electron transfer process to **Fe–TMA** unit. After excitation at 450 nm and in water solution, the GSB of the **$CuInS_2$** QD dynamics was probed at 480 nm. The multi–exponential fit of the black trace in Figure 4c, corresponding to the decay of the MPA-capped **$CuInS_2$** QD, produced six time constants. Two ultrafast electron trapping processes (0.5 and 5 ps) to the lattice and surface sites and four radiative recombination processes (1.7, 5, 38, and 190 ns) from band–edge and mid band gap electrons and holes. In the presence of 0.5 equivalent of **Fe–TMA**, the decay of the band (red trace in Figure 4c) was faster, indicating the existence of an electron transfer process to the **Fe–TMA** unit. The fit of the new absorption decay (red trace in Figure 4c) yielded only three times constants (3 ps (22%), 40 ps (22%), and 800 ps (56%)) for the electron transfer. The transfer processes with sub-picosecond time constant were not

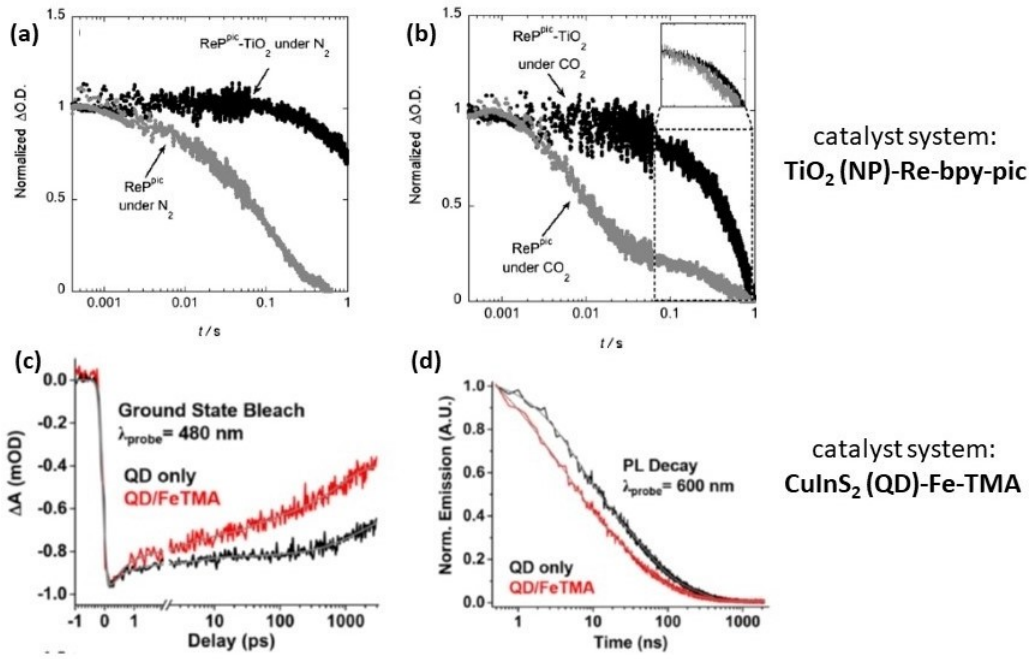

Figure 4. Transient absorption decays of the reduced intermediate **Re**–$\mathbf{P_{pic}}^-$ in DMF containing 1 M TEOA as hole scavenger recorded at 500 nm after 415 nm excitation, (a) **Re**–**bpy**–**pic** in solution (grey) and $\mathbf{TiO_2}$–**Re**–**bpy**–**pic** (black) under N_2, and (b) **Re**–**bpy**–**pic** in solution (grey) and $\mathbf{TiO_2}$–**Re**–**bpy**–**pic** (black) under CO_2; (c) Transient absorption decays of MPA-capped $\mathbf{CuInS_2}$ QD in water with (red) and without (black) 0.5 equivalent of **Fe**–**TMA**, probed at 480 nm (QD Ground state bleach) after excitation at 450 nm; (d) Photoluminescent (PL) decay of MPA–capped $\mathbf{CuInS_2}$ QD in water with (red) or without (black) 0.5 equivalent of **Fe**–**TMA** added, probed at 600 nm, after excitation at 450 nm. Panels (a) and (b), used with permission from C. D. Windle, E. Pastor, A. Reynal, A. C. Whitwood, Y. Vaynzof, J. R. Durrant, R. N. Perutz, E. Reisner, Improving the Photocatalytic Reduction of CO_2 to CO through Immobilisation of a Molecular Re Catalyst on TiO_2. *Chem.–Eur. J.* **2015**, *21*, 3746–3754. Copyright 2015 John Wiley and Sons. Panels (c) and (d) adapted with permission from S. Lian, M. S. Kodaimati, E. A. Weiss, Photocatalytically Active Superstructures of Quantum Dots and Iron Porphyrins for Reduction of CO2 to CO in Water *ACS Nano* **2018**, *12*, 568–575. Copyright 2018 American Chemical Society.

detected. The PL decay measured by means of TCSPC study in a 500 ps to 10 μs window (Figure 4d) showed 50% quenching of the PL for the QD unit. This result confirmed the existence of a donor–acceptor type electronic communication between the $\mathbf{CuInS_2}$ QD and the **Fe**–**TMA** unit. The origin of the heterogeneity of the electron transfer dynamics (three constants) in the $\mathbf{CuInS_2}$–**Fe**–**TMA** hybrid–system was hypothesized to be caused by aggregation of the QDs and the uneven distribution of the **Fe**–**TMA** units on their surfaces.

The charge accumulation of the Co^I species (potent species for catalysis) caused by a double reduction process in the $\mathbf{TiO_2}$–**Co**–**cob** (Co^{III}) system was monitored by TAS. The absorption decay was recorded at 700 nm in acetonitrile solution (containing 0.1 M TEOA) under 355 nm laser excitation.[18b] Without applied external bias, the signal of $\mathbf{TiO_2}$–**Co**–**cob** exhibited a negative slope in the early timescales (~μs) followed by a change in slope at longer timescales (ms-s) (Figure 5b, black trace). The authors suggested that the negative signal at 700 nm corresponded to the bleaching of Co^I species (as they strongly absorb at 700 nm). This observation was indicative of faster accumulation of Co^I species at the TiO_2 surface under open circuit condition. Under prolonged irradiation, the negative signal trace was assigned to a charge recombination pathway via rapid oxidation of the Co^I species to Co^{II} species promoted by the VB (holes). The positive signal observed at longer times was assigned to the re-reduction of the Co^{II} species to Co^I counterparts by CB electrons of the TiO_2. For the $\mathbf{TiO_2}$–**Co**–**ter** system, a similar transient absorption study was performed by monitoring the transient absorption at 550 nm under 355 nm laser excitation (Figure 5c).[18b] Unlike the $\mathbf{TiO_2}$–**Co**–**cob** case, the transient absorption signal for the $\mathbf{TiO_2}$–**Co**–**ter** hybrid catalyst remained similar when recorded with or without applied bias; this aspect is discussed in more detail later. $\mathbf{TiO_2}$–**Co**–**cob** and $\mathbf{TiO_2}$–**Co**–**ter** systems were exclusively explored for the proton reduction study (HER). We don't have any data to comment on the efficiency of the doubly reduced Co^I species towards CO_2RR.

For the $\mathbf{TiO_2}$–**Fe**–**Por** and $\mathbf{TiO_2}$–**Hemin**, the transient absorption measurements were conducted in acetonitrile, with laser excitation at $\lambda = 355$ nm and probed at $\lambda = 680$ nm.[20] The transient signals for $\mathbf{TiO_2}$–**Fe**–**Por** are shown in Figure 6a (green and blue trace); the comparison of transient absorption decays recorded under N_2 atmosphere clearly showed that the $\mathbf{TiO_2}$–**Fe**–**Por** hybrid assemblies exhibited 100 times faster decays (μs-ms) than bare $\mathbf{TiO_2}$ films (ms-s). In the presence of CO_2, the transient absorption signal of $\mathbf{TiO_2}$–**Fe**–**Por** was not markedly affected (green and blue trace in Figure 6a). It was hypothesized that the faster signal decay observed for the $\mathbf{TiO_2}$–**Fe**–**Por** hybrid–assembly corresponded to a back–electron transfer process from the $\mathbf{TiO_2}$ conduction band to an oxidised iron-porphyrin cationic state. It was not related to any charge transfer process involving the CO_2 molecule. $\mathbf{TiO_2}$–**Hemin** showed similar but less intense transient absorption signals in the μs-ms regions and delivered related features in the photoelectrochemically catalyzed CO_2RR; readers are directed to the reference

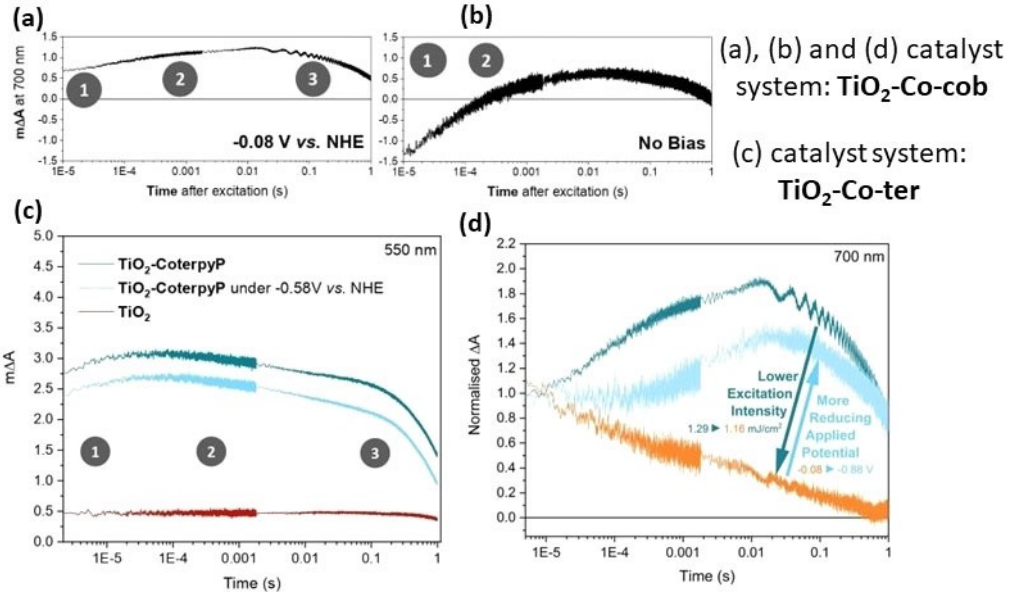

Figure 5. Transient absorption decays of **TiO_2–Co–cob** in acetonitrile containing 0.1 M $TBAPF_6$ and 0.1 M TEOA recorded at 700 nm after 355 nm excitation (a) applied potential (−0.08 V vs. NHE), (b) without applied potential in the same conditions. (c) Transient absorption decays of **TiO_2–Co–ter** and **TiO_2** in acetonitrile containing 0.1 M $TBAPF_6$ and 0.1 M TEOA recoded at 550 nm after 355 nm excitation under with and without applied potential (−0.58 V vs. NHE). The different processes (1–3) taking place at different time scales, which are not shown here. (d) Kinetics of the transient absorption decays of **TiO_2–Co–cob** at 700 nm under different light intensities and applied bias. Panels (a), (b), (c) and (d) are reproduced from C. Bozal–Ginesta, C. A. Mesa, A. Eisenschmidt, L. Francàs, R. B. Shankar, D. Antón–García, J. Warnan, J. Willkomm, A. Reynal, E. Reisner; J. R. Durrant, Charge accumulation kinetics in multi–redox molecular catalysts immobilised on TiO_2. *Chem. Sci.* **2021**, *12*, 946–959 with permission from the Royal Society of Chemistry.

article for the detailed spectra.[20] Considering the energetics of the VB and CB of **TiO_2** and the possible different redox states of the iron porphyrins ($Fe^{III/II}$, $Fe^{II/I}$, $Fe^{I/0}$), it's unlikely to achieve the $Fe^{I/0}$ state (potent for CO_2 reduction) by transferring electrons from the **TiO_2** CB (ideal case of having multi redox events with only photoexcited electrons). In addition, electron transfer from the photo-excited iron porphyrins to the **TiO_2** CB becomes thermodynamically favourable, making Fe-porphyrin based hybrid systems less efficient for CO_2RR. A complete picture of the interfacial charge transfer processes occurring in such **TiO_2–Fe–porphyrin** hybrid assemblies demands a fs-s timescale TAS study, which to date has not been reported.

4.3. Effect of the applied external bias

Under photoelectrochemical conditions, an external bias was applied to the hybrid systems behaving as photocathode and they were subjected to the CO_2RR. For the **TiO_2–Co–cob** system, the transient absorption kinetics were measured under −0.08 V vs NHE applied bias keeping all other conditions identical to the non–voltage biased case.[18b] The resulting transient spectrum measured at the 10 μs to s timescale showed different kinetics in the voltage biased and non–biased experiments (Figure 5a, black trace). Strikingly, under photocatalytic conditions at −0.08 V vs NHE condition, we observed positive signals throughout the complete timescale. A plausible inference of this results was that, under voltage bias condition, the singly reduced Co^{II} species accumulated in the initial timescale. At longer time scales (ms-s), this initially formed species were successively reduced to the doubly reduced state producing Co^{I} species. For **TiO_2–Co–ter**, upon light irradiation under −0.58 V vs NHE applied bias, the transient signal showed a reduced initial transient absorption value. Still, the decays remained similar to the non–bias case (Figure 5c).[18b] Electrochemical studies conducted at different applied biases, confirmed that **TiO_2–Co–ter** underwent two successive electron transfer from the **TiO_2** CB to **Co^{III}**–unit yielding the doubly reduced Co^{I} species at the μs time scale. In the **TiO_2–Co–ter** case, the accumulation of the singly reduced species (Co^{II}) was not detected. This is in striking contrast with the observations made for the **TiO_2–Co–cob** case. The differences in charge accumulation behaviours of **TiO_2–Co–cob** and **TiO_2–Co–ter** hybrid assemblies were attributed to their different $Co^{III/II}$ and $Co^{II/I}$ redox value energies of the attached Co-polypyrrolic complexes in relation to the energy of the **TiO_2** CB.

The transient decays of the **TiO_2–Fe–Por** and **TiO_2–Hemin** systems were recorded from 0 to −1.3 V (vs Ag/AgCl) applied voltage bias and under N_2 and CO_2 atmosphere without added TEOA.[20] A comparison of the transient absorption values at a time of 1×10^{-5} s revealed, that for potentials more negative than −0.8 V the signals disappeared due to the continuum electrochemical filling of electrons from the VB to CB of TiO_2. The comparison of the transient decays at −0.5 V (vs Ag/AgCl) for **TiO_2** and **TiO_2–Fe–Por** is shown in Figure 6b. For **TiO_2–Fe–Por**, it is clear that there were no marked differences in the decays of the experiments performed in N_2 and CO_2 atmosphere. Similar results were obtained in related non-voltage biased experiments (Figure 6b, green and blue trace). Thus, it can be concluded that the decay of the signals (μs-ms timescale) corresponding to the electron transfer from the **TiO_2** CB to the oxidised iron-porphyrin cationic state remain unaffected upon applying the voltage bias. However, the identification of the

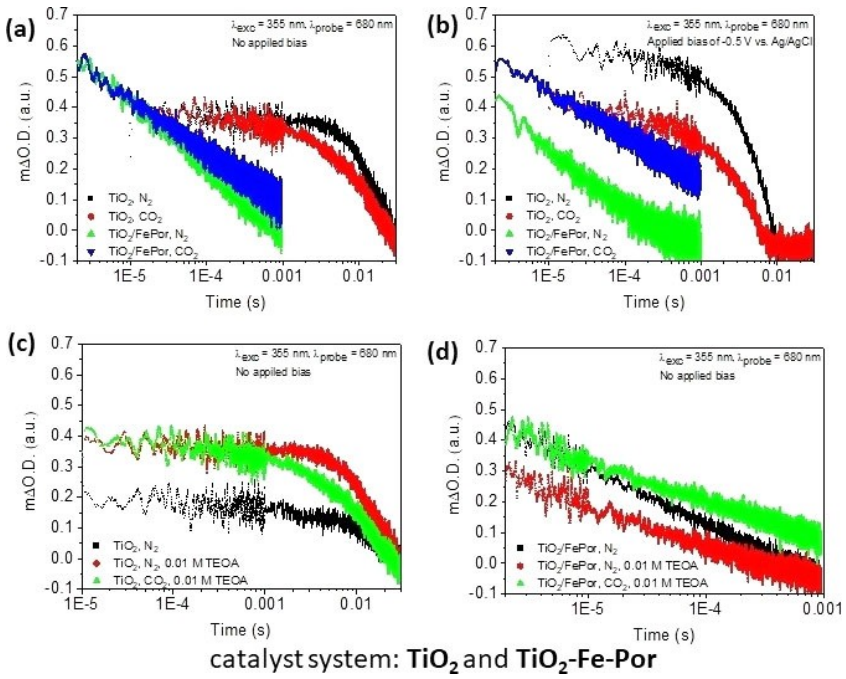

Figure 6. Transient absorption decays of **TiO_2**–**Fe**–**Por**, and **TiO_2** in acetonitrile containing 0.1 M $TBAPF_6$ recorded at 680 nm after 355 nm excitation (a) under N_2 and CO_2 atmosphere and without applied potential, (b) under N_2 and CO_2 atmosphere and applied potential (−0.5 V vs. Ag/AgCl). For both (a) and (b) the spectra of **TiO_2** were only recorded in presence of 0.01 M TEOA as a hole scavenger. (c) and (d) The effect of the hole scavenger (0.01 M TEOA) on **TiO_2** and **Fe**–**Por**, TEOA causes an increase in the transient absorption signal in the case of **TiO_2**. Panels (a), (b), (c) and (d) were adapted, with permission of the authors, from B. Domingo-Tafalla, T. Chatterjee, F. Franco, J. Perez Hernandez, E. Martinez-Ferrero, P. Ballester, E. Palomares, Electro- and Photoinduced Interfacial Charge Transfers in Nanocrystalline Mesoporous TiO_2 and TiO_2/Iron Porphyrin Sensitized Films under CO_2 Reduction Catalysis. *ACS Appl. Mater. Interfaces* **2023**, *15*, 14304–14315 made available under Creative Commons license (CC-BB-NC-ND 4.0) 2023 American Chemical Society.

catalytically active redox state of the Fe in the film resulting from the charge transfer events still needs to be addressed. An indirect proof of the formation of the same species for Fe reduction in the hybrid assembly (**Fe^{III}**–**Por**) with and without applied voltage bias (0 to −1 V vs Ag/AgCl) was deduced from the analogous conversion of CO_2 to CO. The CO_2RR is believed to proceed through Fe(0) oxidation states. Nevertheless, in-situ spectroelectrochemical studies are needed to prove the existence of reduced Fe species (Fe^{I} and Fe^{0}) in the films under the specified reactions conditions.

4.4. Effect of hole scavenger agent

The transient absorption studies described here used triethanolamine (TEOA) as hole scavenger agent except for the **$CuInS_2$** QD. As discussed previously, TEOA was used in high excess (0.1 to 0.01 M in acetonitrile) and helped to obtain better transient absorption values. For example, in bare **TiO_2**, we observed an almost 50% increase in the transient absorption value (ΔO. D) due to the addition of TEOA (black and red colour trace in Figure 6c). In contrast, there was no marked effect on the TAS signals recorded for **TiO_2**–**Fe**–**Por** with or without added **TEOA** (black and red trace in Figure 6d).[20] This observation indicated that, unlike bare **TiO_2**, the use of TEOA as hole scavenger did not affect the stabilisation of Fe porphyrin cationic states. In conclusion, the effect of the hole scavenger agent is specific for the catalysts or hybrid catalysts system, as well as for the process causing the transient absorption signal. Furthermore, the presence of **TEOA** could also affect the CO_2 reduction catalysis, product selectivity, etc.[38] Hence, a careful investigation of the TAS studies and the results of the catalysis experiments under identical condition is mandatory for a sound understanding of the effect of hole transfer agents in solution.

4.5. Effect of the trap states of the semiconductor

Surface states of mesoporous metal oxide semiconductor films (e.g., TiO_2, NiO, etc.) can trap electrons and possess particularly differing properties from those of the bulk.[26,39] Upon photo–excitation, excited electrons from the CB of the semiconductor can get trapped within low–energy surface states. (process **3** in Figure 2a). During photoelectrochemical CO_2RR, under applied reductive external bias voltage, a prolonged accumulation of charges in such trap states significantly influences the multi–redox events of the molecular catalyst unit. For example, a comparative study of electron mobility and transport dynamics in thin films of dye-sensitized TiO_2, ZnO, and SnO_2 nanoparticles displayed the dictating role of trap states in the observed processes.[40] For example, in pristine NiO–based *p*-DSCs, the charge transport behaviour exhibited exponential dependence on light intensity and on the concentration of surface trap states.[41] Studies on **TiO_2**–**Co**–**cob** were carried out to correlate the dependency of the external bias and light intensity on charge accumulation. Monitoring transient decays at 700 nm (deep blue and orange trace in Figure 5d), it was observed that going from high (1.29 mJ cm^{-2}) to low (1.16 mJ cm^{-2}) intensity laser excitation, the accumulation of the mono to doubly reduced **Co^{III}**–**cob** catalyst

species at the electrode decreased (apparent quantum yield of Co^{II} to Co^{I} species at 700 nm decreased from 44% to 1%). The concentration of doubly reduced species can be regained again by applying external bias voltages, which fill up the trap states electrochemically.[18b] After applying −0.88 V vs. NHE and at low excitation energy, the kinetics at 700 nm (sky blue trace in Figure 5d) can be partially regained (the apparent quantum yield increased to 22%), similar to the experiment performed with high–intensity laser excitation. To our knowledge, a detailed study correlating the role of trap states with charge transfer kinetics and the performance of CO_2 reduction catalysis is still lacking.

5. Conclusions and Perspectives

In this mini–review, we summarized recent developments regarding interfacial charge transfer studies in semiconductor-molecular catalyst hybrid assemblies for photo- and photoelectrochemically induced CO_2RR. The efficiency of the multi–redox–driven hybrid catalysts dramatically depends on the favourable transport of the photogenerated electrons from the light–harvesting photosensitizer (semiconductor) to the metal reaction centre. A challenge in this area is to ensure good stability of the hybrid catalyst assemblies and maximum interfacial charge transfer processes in favour of catalysis. Interfacial charge transfer processes occur on ultrafast to fast time scales (fs-ms), whereas catalysis happens on a much lower time scales (μs-ms). Charge recombination in bulk semiconductors and back electron recombination taking place at the interfaces are also faster than the catalysis processes. The two recombination processes are detrimental to interfacial charge transfer and disfavours the multi–redox based reduction reaction at the molecular catalyst unit. At the interface of the hybrid assembly with the electrolyte solution the applied potential and the alignment of the energy states of the hybrid assemblies are drastically affected by band bending, electron filling of the surface states, etc. As a result, the interfacial charge transfer processes are sensitive to the structure of the hybrid assembly, the pH of the solution, the intensity of the light irradiation, the CO_2 feeding source, the applied potential and other aspects of the CO_2RR conditions. Hence, characterising the interfacial charge transfer processes by ultrafast spectroscopy and identifying the processes ranging from fs to ms timescale is crucial. The examples discussed here included mesoporous TiO_2 film, TiO_2 nanoparticle, $CuInS_2$ quantum dots, as light harvesting semiconductors, which are covalently or supramolecularly functionalised with Co-polypyrrolic complexes, Fe-porphyrins, and Re-bipyridine complexes, as active catalytic sites. The best results were obtained with the **$CuInS_2$–Fe–TMA** hybrid assembly which furnished the CO_2 reduction to CO at $\lambda = 450$ nm excitation in water. TAS study confirmed that there was a donor–acceptor type electronic communication between the **$CuInS_2$** QD and the **Fe–TMA** unit featuring three different times constants (3 ps (22%), 40 ps (22%), and 800 ps (56%)) for the electron transfer dynamics. All together, these examples allowed us to gain some insights on the catalysis and the associated charge transfer dynamics operating in such systems. Still, more operando spectroelectrochemical studies are necessary to have a better understanding the correlation between charge transfer dynamics and catalysis. This is especially the case considering that despite the large number of reports on different CO_2 reduction catalysis systems, the number of reports addressing interfacial charge transfer studies on those systems are scarce. Indeed, the large complexity of the charge transfer processes occurring in hybrid systems is high enough to led us conclude that realistically mimicking the blueprint of natural photosynthesis in technologically relevant materials is not at our reach in a short period of time. However, the current findings support development of superior CO_2 reduction photoelectrodes with a proper choice of materials, thickness of the layers, molecular catalyst attachment, charge transfer from semiconductor CB to molecular catalyst unit. Solar to chemical energy conversion can be efficiently improved using artificial catalysts for CO_2RR by tuning the interfacial charge transfer processes. Future work should aim to progress from fundamental aspects of heterogeneous photochemistry to interfacial aspects of heterojunctions by correlating interfacial charge transfer with catalysis performance.

Probably, one of the best strategies to increase the stability of anchored molecular catalysts on semiconductor surfaces under the CO_2RR condition could be accessing reticular chemistry. That is, exploiting the potential of combining molecular complex with reticular materials. Taking advantage of the recent progress achieved in the synthesis and characterisation techniques of metal organic frameworks (MOFs) and covalent organic frameworks (COFs), it is sensible to consider growing/linking 'in situ' or through photosynthetic modifications the functionalised molecular catalyst on the semiconductor. This approach would provide a precise molecular–level control in the assembly of the hybrid material containing a metal catalytic centre with flexible organic linkers and semiconductors with long–lived charge–separated properties. Moreover, tailoring the assembly of semiconductor and the molecular catalysts is crucial in controlling most of the interfacial charge transfer processes. Doping the semiconductor with suitable elements and synthetically installing electron–withdrawing or donor groups in the ligand of the molecular catalyst could guide to a better hybrid assembly with a broader region of absorption in the solar spectrum and high turnovers. Other potential improvements include detailed investigations on the trap/surface states of the semiconductor, which could provide new insights into the electronic and catalytic properties of the hybrid catalyst systems. Considering all the complex and vital factors that lie behind the design of the hybrid catalytic system, focusing on the interfaces is mandatory in order to establish a meaningful correlation between catalysis efficiency and charge transfer dynamics. We hope this mini–review will contribute to the current understanding of interfacial processes at play during the light–assisted CO_2 reduction studied in different semiconductor–molecular catalyst–based systems. We expect that it will also encourage the Solar Fuel community to investigate the favourable and detrimental charge transfer pathways in the newly-designed catalyst systems.

Acknowledgements

The authors thank all the research groups who contributed to probing interfaces using ultrafast spectroscopy during the photo–induced CO_2 reduction. T. C. acknowledges Beatriu de Pinós 2021

grant from the Government of Catalunya AGAUR (2021-BP-00204). B. D.-T. thanks to MICINN and ESF, for a predoctoral grant (PRE2020-092525). E. P. and P. B gratefully acknowledge financial support from ICIQ, MICINN (PID2022-139866NB–I00 and PID2020-114020GB–I00), Severo Ochoa Grant MCIN/AEI/10.13039/501100011033 (CEX2019-000925-S) the CERCA Programme/Generalitat de Catalunya, AGAUR (2021SGR00851 and 2021SGR01261) and ICREA. Funding from the NEFERTITI project (H2020, Grant agreement ID: 101022202) is also acknowledged.

Conflict of Interests

The authors declare no conflict of interest.

Data Availability Statement

Data sharing is not applicable to this article as no new data were created or analyzed in this study.

[1] D. G. Nocera, *Acc. Chem. Res.* **2012**, *45*, 767–776.
[2] a) R. E. Smalley, *MRS Bull.* **2005**, *30*, 412–417; b) N. S. Lewis, D. G. Nocera, *Proc. Natl. Acad. Sci. USA* **2006**, *103*, 15729–15735.
[3] a) E. S. Andreiadis, M. Chavarot-Kerlidou, M. Fontecave, V. Artero, *Photochem. Photobiol.* **2011**, *87*, 946–964; b) L. Hammarström, S. Hammes-Schiffer, *Acc. Chem. Res.* **2009**, *42*, 1859–1860.
[4] *Photosynthesis, McGraw-Hill Encyclopedia of Science and Technology,* 10th edn, *Vol. 13. New York: McGraw-Hill* **2007** pp 468–475.
[5] a) R. E. Blankenship, et. al, *Science* **2011**, *332*, 805–809; b) B. A. Sowjanya, B. D. Narayana, S. Shreyas, *Int.J.Curr.Microbiol.App.Sci* **2019**, *8*, 775–786.
[6] a) C. Liu, B. C. Colón, M. Ziesack, P. A. Silver, D. G. Nocera, *Science* **2016**, *352*, 1210–1213; b) M. D. Karkas, O. Verho, E. V. Johnston, B. Åkermark, *B. Chem. Rev.* **2014**, *114*, 11863–12001.
[7] M. Robert, *ACS Energy Lett.* **2016**, *1*, 281–282.
[8] a) H. Kumagai, Y. Tamaki, O. Ishitani, *Acc. Chem. Res.* **2022**, *55*, 978–990; b) T. Morikawa, S. Sato, K. Sekizawa, T. M. Suzuki, T. Arai, *Acc. Chem. Res.* **2022**, *55*, 933–943; c) L. Liu, Z. Wang, J. Zhang, O. Ruzimuradov, K. Dai, J. Low, *Adv. Mater.* **2023**, *35*, 2300643.
[9] Q. Xu, Z. Xia, J. Zhang, Z. Wei, Q. Guo, H. Jin, H. Tang, S. Li, X. Pan, Z. Su, S. Wang, *Carbon Enrgy* **2023**, *5*, e205.
[10] a) S. Lian, M. S. Kodaimati, D. S. Dolzhnikov, R. Calzada, E. A. Weiss, *J. Am. Chem. Soc.* **2017**, *139*, 8931–8938; b) F. Arcudi, L. Đorđevíc, B. Nagasing, S. I. Stupp, E. A. Weiss, *J. Am. Chem. Soc.* **2021**, *143*, 18131–18138; c) H. .-L. Wu, X. .-B. Li, C. .-H. Tung, L. .-Z. Wu, *Adv. Mater.* **2019**, *31*, 1900709.
[11] a) D. Khusnutdinova, A. M. Beiler, B. L. Wadsworth, S. I. Jacob, G. F. Moore, *Chem. Sci.* **2017**, *8*, 253–259; b) B. Kumar, J. M. Smieja, C. P. Kubiak, J. Phys, *Chem. C.* **2010**, *114*, 14220–14223.
[12] X. Wang, C. Li, *Journal of Photochemistry and Photobiology C: Photochemistry Reviews* **2017**, *33*, 165–179.
[13] V. Kumaravel, J. Bartlett, S. C. Pillai, *ACS Energy Lett.* **2020**, *5*, 486–519.
[14] H. Takeda, C. Cometto, O. Ishitani, M. Robert, *ACS Catal.* **2017**, *7*, 70–88.
[15] a) E. Boutin, L. Merakeb, B. Ma, B. Boudy, M. Wang, J. Bonin, E. Anxolabéhère Mallart, M. Robert, *Chem. Soc. Rev.* **2020**, *49*, 5772–5809; b) B. Domingo-Tafalla, T. Chatterjee, E. Palomares, *J. Porphyrins Phthalocyanines* **2023**, *27*, 23–46.
[16] D. A. Garcia Osorio, G. Neri, A. J. Cowan, *ChemPhotoChem* **2021**, *5*, 595–610.
[17] a) A. Reynal, F. Lakadamyali, M. A. Gross, E. Reisner, J. R. Durrant, *Energy Environ. Sci.* **2013**, *6*, 3291–3300; b) A. Reynal, J. Willkomm, N. M. Muresan, F. Lakadamyali, M. Planells, E. Reisner, J. R. Durrant, *Chem. Commun.* **2014**, *50*, 12768–12771.
[18] a) C. D. Windle, E. Pastor, A. Reynal, A. C. Whitwood, Y. Vaynzof, J. R. Durrant, R. N. Perutz, E. Reisner, *Chem. Eur. J.* **2015**, *21*, 3746–3754; b) C. Bozal-Ginesta, C. A. Mesa, A. Eisenschmidt, L. Francàs, R. B. Shankar, D. Antón-García, J. Warnan, J. Willkomm, A. Reynal, E. Reisner, J. R. Durrant, *Chem. Sci.* **2021**, *12*, 946–959.
[19] S. Lian, M. S. Kodaimati, E. A. Weiss, *ACS Nano* **2018**, *12*, 568–575.
[20] B. Domingo-Tafalla, T. Chatterjee, F. Franco, J. P. Hernandez, E. Martinez-Ferrero, P. Ballester, E. Palomares, *ACS Appl. Mater. Interfaces* **2023**, *15*, 14304–14315.
[21] M. Grätzel, *Nature* **2001**, *414*, 338–344.
[22] a) W. H. Brattain, C. G. B. Garrett, *Bell Syst. Tech. J.* **1955**, *34*, 129–176; b) H. Gerischer, *J. Electrochem. Soc.* **1966**, *113*, 1174–1182; c) R. A. Marcus, *J. Chem. Phys.* **1965**, *43*, 679–701.
[23] A. J. Nozik, *Annu. Rev. Phys. Chem.* **1978**, *29*, 189–222.
[24] Z. Zhang, J. T. Yates, *Chem. Rev.* **2012**, *112*, 5520–5551.
[25] A. J. Bard, F.-R. F. Fan, A. S. Gioda, G. Nagasubramanian, H. S. White, *Faraday Discuss. Chem. Soc.* **1980**, *70*, 19–31.
[26] J. L. White, M. F. Baruch, J. E. Pander, Y. Hu, I. C. Fortmeyer, J. E. Park, T. Zhang, K. Liao, J. Gu, Y. Yan, T. W. Shaw, E. Abelev, A. B. Bocarsly, *Chem. Rev.* **2015**, *115*, 12888–12935.
[27] P. Hutchison, C. J. Kaminsky, Y. Surendranath, S. Hammes-Schiffer, *ACS Cent. Sci.* **2023**, *9*, 927–936.
[28] J. M. Mayer, *J. Am. Chem. Soc.* **2023**, *145*, 7050–706.
[29] N. D. Keller, P. Vecchi, D. C. Grills, D. E. Polyansky, G. P. Bein, J. L. Dempsey, J. F. Cahoon, G. N. Parsons, R. N. Sampaio, G. J. Meyer, *J. Am. Chem. Soc.* **2023**, *145*, 11282–11292.
[30] H.-J. Son, C. Pac, S. O. Kang, *Acc. Chem. Res.* **2021**, *54*, 4530–4544.
[31] H. Mandal, M. Chakali, M. Venkatesan, P. R. Bangal, *J. Phys. Chem. C* **2021**, *125*, 4750–4763.
[32] X. Wang, A. Kafizas, X. Li, S. J. A. Moniz, P. J. T. Reardon, J. Tang, I. P. Parkin, J. R. Durrant, *J. Phys. Chem. C.* **2015**, *119(19)*, 10439–10447.
[33] Y. Pellegrin, F. Odobel, *C. R. Chim.* **2017**, *20*, 283–295.
[34] a) Y. Tamaki, A. Furube, R. Katoh, M. Murai, K. Hara, H. Arakawa, M. Tachiya, *C. R. Chim.* **2006**, *9*, 268–274; b) A. J. Cowan, J. R. Durrant, *Chem. Soc. Rev.* **2013**, *42*, 2281–2293; c) J. Huang, D. Stockwell, Z. Q. Huang, D. L. Mohler, T. Q. Lian, *J. Am. Chem. Soc.* **2008**, *130*, 5632–5633.
[35] a) X. Wang, Z. Feng, J. Shi, G. Jia, S. Shen, J. Zhou, C. Li, *Phys. Chem. Chem. Phys.* **2010**, *12*, 7083-7090; b) A. Pal, S. Srivastava, R. Gupta, S. Sapra, *Phys. Chem. Chem. Phys.* **2013**, *15*, 15888–15895.
[36] A. Trapali, P. Gotico, C. Herrero, M.-H. Ha-Thi, T. Pino, W. Leibl, G. Charalambidis, A. Coutsolelos, Z. Halime, A. Aukauloo, *C. R. Chim.* **2021**, *24*, 101–114.
[37] S. Rodríguez-Jiménez, H. Song, E. Lam, D. Wright, A. Pannwitz, S. A. Bonke, J. J. Baumberg, S. Bonnet, L. Hammarström, E. Reisner, *J. Am. Chem. Soc.* **2022**, *144*, 9399–9412.
[38] G. Sahara, O. Ishitani, *Inorg. Chem.* **2015**, *54*, 5096–5104.
[39] X. Chen, S. S. Mao, *Chem. Rev.* **2007**, *107*, 2891–2959.
[40] P. Tiwana, P. Docampo, M. B. Johnston, H. J. Snaith, L. M. Herz, *ACS Nano* **2011**, *5*, 5158–5166.
[41] L. Tian, R. Tyburski, C. Wen, R. Sun, M. Abdellah, J. Huang, L. D'Amario, G. Boschloo, L. Hammarström, H. Tian, *J. Am. Chem. Soc.* **2020**, *142*, 18668–18678.

Manuscript received: October 31, 2023
Revised manuscript received: February 6, 2024
Version of record online: ■■, ■■

REVIEW

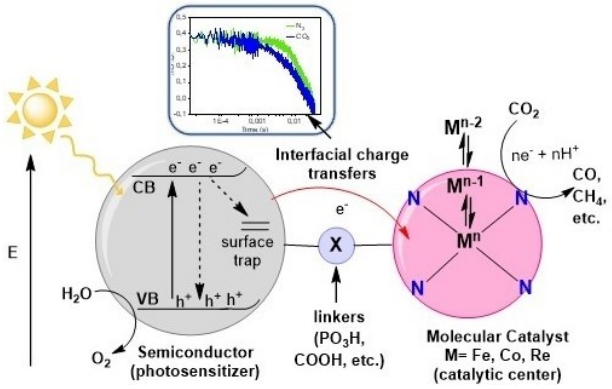

T. Chatterjee, B. Domingo-Tafalla, Prof. P. Ballester*, E. Palomares**

This mini–review describes recent examples of Semiconductor–Molecular catalyst hybrid systems in which complementary studies were performed relating interfacial photo–induced charge transfer measurements and their impact on photo and photoelectrochemical multi–redox CO_2 reduction reactions.